Research Square

Preprints are preliminary reports that have not undergone peer review.
They should not be considered conclusive, used to inform clinical practice,
or referenced by the media as validated information.

Assessment of interkingdom TIR domain interactions using a modular yeast tripartite split-GFP system

Alejandro Fernández-Vega
Universidad Complutense de Madrid
Elba del Val
Universidad Complutense de Madrid
Julia María Coronas-Serna
Universidad Complutense de Madrid
Humberto Martín
Universidad Complutense de Madrid
María Molina
Universidad Complutense de Madrid
Isabel Rodríguez-Escudero
Universidad Complutense de Madrid
Víctor Cid
vicjcid@ucm.es

Universidad Complutense de Madrid

Article

Keywords: split-GFP, yeast, Saccharomyces cerevisiae, TIR domains, Brucella, innate immunity

Posted Date: March 25th, 2026

DOI: https://doi.org/10.21203/rs.3.rs-9032499/v1

License: This work is licensed under a Creative Commons Attribution 4.0 International License.
Read Full License

Additional Declarations: No competing interests reported.

Abstract

Thanks to its genetic resourcefulness, *Saccharomyces cerevisiae* has been traditionally used as a model organism to detect and study protein-protein interactions. The recent development of synthetic biology toolkits brings an opportunity to expand such utilities. Here, we coupled the modular cloning (MoClo) system to the tripartite split-GFP strategy to systematically study protein interactions in particular cellular localizations. To provide proof-of-principle of this yeast-based tripartite split-GFP (ytpGFP), we challenged interactions of bacterial TIR domain-containing proteins (*Brucella* BtpA and BtpB) between themselves, as well as against human TIR adaptors of the myddosome and triffosome innate immune signaling complexes. While fluorescence microscopy provided clues about which member of the interacting pair drives subcellular localization of the complex, interactions could be readily tracked and quantified by flow cytometry. The ytpGFP system detected known homotypic or heterotypic complexes and defined previously unknown interkingdom TIR-TIR interactions. Human MyD88, TIRAP, TRAM, and TRIF were capable of interacting with both BtpA and BtpB TIR domains. Furthermore, our results suggest that the N-terminal non-TIR extensions of both BtpA and, especially, BtpB limit the ability of their TIR domains to interact. This strategy is a useful addition to other yeast-based tools to study protein complexes.

Introduction

Saccharomyces cerevisiae has served as a key model for genetic and genomic studies over the last decades. Its engineering has begotten multiple tools, thus becoming an attractive chassis for synthetic biology [1, 2]. Some of the strategies devised in baker's yeast have widely contributed to define protein-protein interactions, a paramount example being the yeast two-hybrid system [3, 4]. The recent development of split-GFP systems has added a new dimension to the study of protein-protein interactions *in vivo*. Beyond the detection of sheer protein-protein interaction or co-existence of proteins within complexes, it provides spatial information on the subcellular compartment in which the interactions under study take place [5]. One of such strategies is the tripartite split-GFP, in which the interacting proteins bear individual β-sheets of GFP in a cellular system expressing an incomplete GFP structure that will only be reconstituted upon interaction of the proteins tested [6]. The tripartite GFP system was first used in *S. cerevisiae* by the Thorner lab to titrate interactions among septins [7]. Here we propose its adaptation to the MoClo synthetic biology toolkit in this model organism [8] for systematic studies on protein-protein interactions and the subcellular localization of assembled protein complexes.

Cell signaling pathways in innate immunity are key to maintain homeostasis and to recognize the presence of both pathogens and cell damage. Their function often relies on the assembly of supramolecular organizing centers (SMOCs) that transmit and amplify the signal after receptor stimulation [9]. Toll-like receptor (TLR) pathways are paradigmatic in innate immune signaling, assembling SMOC signalosomes named myddosomes, which contain the core adaptor MyD88, or triffosomes, which include the core adaptor TRIF [10, 11]. Interactions between TLRs and their adaptors

to build SMOCs are sustained by homo- and heterotypic interactions mediated by their Toll-Interleukin-1 Receptor (TIR) domains. Such interactions are essential to trigger innate immune signaling in response to TLR activation by pathogen-associated ligands.

The TIR fold is not exclusive to innate immune pathways in vertebrates: it is also found in plants, as part of their immune system, and in bacteria, probably as an anti-phage system. Bacterial TIR domains often display enzymatic activities, using nicotinamide adenine dinucleotide (NAD^+) as a substrate to generate second messenger metabolites or to regulate energy metabolism [12, 13]. Some pathogenic bacteria, like uropathogenic *Escherichia coli*, *Pseudomonas aeruginosa*, *Staphylococcus aureus* or *Brucella sp.* express TIR domain-containing proteins that are thought to contribute to host-cell hijacking and innate immune evasion during infection [14–17]. *Brucella* encodes two Type IV secretion system (T4SS)-translocated effector proteins containing a TIR domain: BtpA (also known as TcpB) and BtpB. They have been reported to downregulate the TLR4 signaling pathways triggered by bacterial lipopolysaccharide (LPS) by interfering with TLR4-TIRAP-MyD88 interactions during myddosome formation [18–27]. Nevertheless, the precise interactions that take place between bacterial and mammalian TIRs remain controversial. We have chosen *Brucella* BtpA and BtpB TIR-mediated self-interactions, as well as heterotypic bacterial Btp-human TIR to test proof-of-concept of MoClo-adapted tripartite split-GFP system in yeast and shed light on the nature and cellular location of such interactions.

Results

Adaptation of the tripartite split-GFP system to the MoClo platform

To systematically evaluate protein-protein interactions of sets of TIR domain-containing proteins in a ready yeast-based system, we chose the tripartite GFP system [28], which had been previously set up in the yeast model [7]. With this aim, we decided to adapt this system to the modular cloning (MoClo) Synthetic Biology toolkit [29]. Briefly, tripartite split-GFP relies on reconstitution of the 11 β-sheet barrel structure of GFP by co-expressing an incomplete β1–9 barrel, which will only produce fluorescence when the missing β10 and β11 sheets are co-produced in the cell. The fusion of each β-sheet to two different proteins will yield GFP fluorescence only if those two proteins are found in proximity, both in time and space [28]. Supplementing the MoClo system with appropriate extra part vectors that allow the construction of GFP β10 and β11, both as N- and C-terminal fusions in yeast expression vectors, should provide a useful and reliable tool to systematically test interactions between protein pairs.

First, we generated a yeast strain with the incomplete GFP barrel sequence (GFP β1–9) integrated upstream the *HO* gene. This was done by forcing homologous recombination of a *GAL1/10-GFP(β1–9)-kanMX* cassette, amplified from the pGF-IVL794 plasmid [7]. Additionally, we designed MoClo 3a or 4a Part plasmids to assemble N- or C-terminally tagged, respectively, in-frame GFP β10 or β11 fusions. Thus, for each interaction pair to be tested, the coding sequence in MoClo part 3b could be assembled on either *URA3*- or *HIS3*-based centromeric vectors under the control of the strong inducible *GAL1*

promoter, induced by galactose and repressed by glucose, to regulate protein expression and maximize expression levels (Fig. 1). Furthermore, to easily verify protein expression, we included a 3×FLAG-6×His tag on the terminus opposite to the GFP β-strand. Systematic transformation of all combination pairs of plasmids into the GFP β1–9 engineered yeast strain should produce a fluorescence readout upon positive interaction when shifted to galactose-based medium. We named this setting Yeast TriPartite split-GFP (ytpGFP). Expression of all fusion proteins generated produced was verified by Western blotting with anti-6×His or anti-FLAG antibodies (Supplementary Figure S1).

Assessment of Brucella BtpA and BtpB self-interactions with the ytpGFP system

Brucella BtpA and BtpB are known to downregulate the inflammatory host response by interfering with TIR-TIR interactions at the host signalosomes [19, 20, 23–25], but it has also been reported that both BtpA and BtpB can self-assemble, forming dimers [18, 30]. We have previously shown that the production in yeast cells of their TIR domains alone, devoid of their C-terminal extension, leads to the assembly of long cytoplasmic filaments, while the full-length protein does not [31]. We chose to test Btp self-interaction to validate the ytpGFP system.

Like other bacterial TIR-domains, those in BtpA and BtpB have NAD^+ase activity [12], and their production in yeast leads to severe toxicity due to NAD^+ depletion [31]. Thus, we were prompted to use point mutants $BtpA^{E217A}$ and $BtpB^{E234A}$ in all our experiments. These mutants are deprived of such enzymatic activity, while their ability to form highly ordered filamentous structures of BtpA and BtpB TIR domains is unaffected [31]. We used the ytpGFP assembly to produce both full-length and TIR-domain alone versions of BtpA and BtpB fused to GFP β10 and β11 both N- and C-terminally. We tested self-association by ytpGFP for all homotypic combination pairs. As expected, combinations of any of the Btp constructs with the corresponding control empty vectors bearing only the 3xFLAG-6xHis sequence N-terminally fused to β10 or β11 tag displayed no fluorescence (not shown), but all homotypic BtpA-BtpA and BtpB-BtpB pairs tested showed fluorescence and a characteristic subcellular localization, denoting self-interaction (Fig. 2A-D).

In all combinations, full-length BtpA showed a homogeneous diffuse cytoplasmic fluorescence (Fig. 2A), suggesting that lower order soluble complexes, perhaps dimers [18, 30] were produced. In contrast, removal of the N-terminal extension of BtpA led to the formation of long filamentous, often circular, higher order structures of BtpA(TIR) in all combinations (Fig. 2B). In contrast, full-length BtpB homotypic interaction was manifest as filaments, but only when both strands were placed C-terminally (Ct-Ct); when at least one of the strands was placed in the N-terminus (Nt-Ct or Nt-Ct), spots rather than filaments were observed, which were tighter when both strands were N-terminally fused (Nt-Nt) (Fig. 2C). Finally, removal of the non-TIR N-terminal extension of BtpB led to the formation of BtpB(TIR) filamentous structures in all configurations (Fig. 2D). These observations suggest that the presence of the N-terminal extensions of BtpA and BtpB limit the spontaneous formation of filaments driven by TIR-TIR interactions.

We also tested interactions between full-length Btps and their respective TIR domains alone (Supplementary Figure S2A-B). Peculiarly, all combinations involving one full-length BtpA in the interacting pair maintained a diffuse nucleocytoplasmic pattern and failed to assemble filaments. On the contrary, all full-length BtpB-BtpB(TIR) combinations often formed filamentous structures. To understand this distinct self-association behavior of BtpA and BtpB, we used AlphaFold3 to predict the formation of putative homopolymers ranging from 2 to 6 subunits. While BtpA prediction for a dimer was robust, involving a canonical TIR-TIR interaction (Fig. 3A, left and Supplementary Figure S3A), stable higher order assemblies were not favored (Supplementary Figure S3B and E), likely because BtpA N-terminal α-helices preclude homopolymerization. In contrast, consistent with the aggregative properties observed *in vivo* in our ytpGFP assay, the BtpB N-terminal domains were predicted to fold as a globular structure that cooperated with the TIR domain to assemble stable multimers (Fig. 3A, right), and the probability of interaction according to AlphaFold3 increased as more subunits were added to the prediction (Supplementary Figures S3C-E).

To complement these data with a quantitative output of the interactions, we measured the fluorescent signal of all combinations by flow cytometry. As shown in Fig. 2E, this analysis revealed that BtpB(TIR) self-interaction led to the highest fluorescence intensity, while that of full-length BtpB was the less intense. In contrast, the signal corresponding to full-length BtpA and the BtpA TIR domains alone was similar. The intensity of the signal may be biased by the size of the fluorescent structures (filaments versus spots or diffuse cytoplasmic patterns). Our systematic experimental design allowed to compare all combinations of N-terminally and C-terminally tagged pairs by this means (Fig. 2F). This might provide clues on the topology of the interactions. Moreover, the distance of the linker used between the protein and the GFP strands can be used as a molecular ruler to estimate the distance between the interactors in the complex [7]. In our experiments, we used a 5 amino acid linker for N-terminal constructs and a 10 amino acid linker for C-terminal constructs. Thus, it was expected that C-terminally tagged constructs produced stronger interaction readouts. However, when comparing Nt-Nt vs. Nt-Ct, Ct-Nt or Ct-Ct combinations for each pair, the most intense corresponded to the Nt-Ct pair (Fig. 2F). Rather than reflecting topology aspects, this seemed to correlate with the most efficiently expressed fusions as determined by immunoblot (see Supplementary Figure S1). To visually present an estimate of the efficacy of interaction for each given pair in systematic analyses, we devised a color code, illustrated in the grid in Fig. 3B: a negative interaction both by microscopy and flow cytometry was marked in red; a positive interaction as detected by microscopy, but with a signal below threshold to be detected by flow cytometry, was marked in orange; and those that were significantly over threshold by flow cytometry with different degrees of fold increase were marked in yellow (fluorescence < 2-fold), light green (2- to 5-fold) or dark green (> 5-fold).

Heterotypic BtpA-BtpB interactions are weaker than homotypic assemblies

BtpA and BtpB are evolutionary divergent and share between themselves a low primary sequence homology, even at the TIR domain [24]. We challenged the ytpGFP system to detect heterotypic BtpA-BtpB interactions (Fig. 3B and Supplementary Figures S2C-F). Although the signal was much fainter than that of homotypic interactions shown above, fluorescent intracellular structures could be visualized microscopically in some BtpA-BtpB combinations. Full-length BtpB only led to faint fluorescent spots when tested against BtpA or BtpA(TIR) in the Ct-Ct configuration (Supplementary Figures S2C and F), but this signal was not detected by flow cytometry (Supplementary Figure S2G). All versions of BtpA were recruited to BtpB(TIR) filaments (Supplementary Figures S2D-E), but again the signal was too weak to be detected by flow cytometry (Supplementary Figure S2G). Only some combinations of BtpB(TIR) with full-length BtpA yielded a mild, although reproducible and significant, increase over the basal fluorescence of the control (Supplementary Figure S2G). Hence, heterotypic BtpA-BtpB combinations produced a much weaker signal as compared to that of homotypic ones.

Systematic interaction assay of human TIR adaptors vs. Brucella TIR domains

Next, we endeavoured to use the ytpGFP assay to assess the putative inter-kingdom interaction of both BtpA and BtpB with the TIR-domain containing adaptors in TLR signaling pathways, namely MyD88, TIRAP, TRAM and TRIF. The cDNAs coding for these human proteins were cloned in fusion to the GFP β11-sheet both as N- and C-terminal fusions. Again, a 3×FLAG-6·His tag at the end opposite the GFP β11 sheet to allow immunodetection. Since expression of human TIR adaptor proteins is not toxic for yeast cells [32], they could be safely tested. All constructs were correctly expressed under galactose-induction conditions, as verified by immunoblot on yeast lysates (Supplementary Figure S1C). We assayed all possible combinations between the individual human TIR adaptors and both the NAD^+ase-dead *Brucella* effectors or their isolated TIR domains (all combinations shown in Supplementary Figure S4).

Under the fluorescence microscope, full-length BtpA led to detectable signal with all four human TIR adaptors, while full-length BtpB only showed interaction with MyD88 and TRAM. However, the TIR domains alone of both *Brucella* proteins interacted with all human adaptors at least in one of the N- or C-terminal configurations tested (Fig. 4A and Supplementary Figure S4). Two of the constructs, namely β11-TIRAP and TRIF-β11, although properly expressed (Figure S1C), failed to interact with any partner tested (Supplementary Figure S4).

By using the ytpGFP experimental setting, it can be assessed whether one of the proteins in each interacting pair drags the other into its subcellular localization, implying a ‘spatial dominance’. For example, MyD88 localization seemed dominant over those of full-length or TIR-alone BtpA and BtpB. When heterologously expressed in yeast, MyD88 has been reported to decorate the endoplasmic reticulum-mitochondria encounter structures (ERMES) in a fashion dependent of its N-terminal Death domain (DD) [32, 33], typically concentrating at one or two tight spots per cell, and this is the localization pattern observed in the interactions involving MyD88-β11 (Fig. 4A and Supplementary Figure S4A-B). However, the interactions involving N-terminally tagged β11-MyD88 were detected at short filamentous structures (Supplementary Figure S4), suggesting that the N-terminal tag may affect MyD88 ERMES

localization. TIRAP-β11 showed a dominant localization at the plasma membrane over BtpA, BtpA(TIR) and BtpB(TIR), but failed to interact with full-length BtpB. Thus, the N-terminal extension of BtpB seems to preclude TIRAP-BtpB(TIR) interaction.

Both TRAM-β11 and β11-TRAM constructs were able to interact with all Btp versions, except for β10-BtpB (Fig. 4A and Supplementary Figure S4A-B). In this case, TRAM was mostly recruited to long intracytoplasmic filaments. It is interesting to note that full-length BtpA in both Nt or Ct configurations assembled with TRAM to form such filaments, suggesting that TRAM releases the BtpA TIR domain from the inhibitory effect of its own N-terminal extension on TIR-driven homopolymerization. In contrast, β11-TRIF formed one unique large cytoplasmic spot per cell, to which BtpA, BtpA(TIR) and BtpB(TIR), but not full-length BtpB, were recruited. Thus, dominance of the localization accounts on TRIF, but the N-terminal extension of BtpB seems to outcompete TRIF-BtpB TIR-TIR interaction.

Next, we tested by flow cytometry all Ct-Ct combinations (except for TRIF, for which the Ct fusion was negative, so the Nt β11-TRIF fusion was tested instead). Like heterotypic BtpA-BtpB interactions, these inter-kingdom interactions did not seem as robust as the Btp-Btp homotypic interactions above-described, since the fluorescent signal detected by flow cytometry was weak, leading only to mild shift (less than 2-fold) in fluorescence that yielded statistical significance over the empty vector control in the case of BtpA with TIRAP, BtpA(TIR) with TRAM, and BtpB(TIR) with both TIRAP and TRAM (Fig. 4B and Supplementary Figure S5). Only interactions of the isolated TIR domains of both Btps with TRAM yielded a consistent signal of 1.5 fold over the basal control (Supplementary Figure S5). In sum, the ytpGFP system indicates that both BtpA and BtpB TIR domains have intrinsic ability to interact with all human TIR adaptors *in vivo*.

Discussion

Synthetic biology tools provide powerful and versatile platforms for basic research. In this report we present ytpGFP as a resource to study protein-protein interactions in the yeast model, based on the use of MoClo standardized scaffolds [29] to facilitate systematic assays based on the tripartite split-GFP [6]. Assays based on split-GFP have the advantage over the two-hybrid system that they reveal the subcellular compartments in which the interaction takes place. Furthermore, in the case of proteins involved in the assembly of highly ordered structures, these can be visualized *in vivo* on account of the interaction under study.

Since the TIR fold is a well-known universal protein-protein interaction domain involved in both homo- and heterotypic interactions [11, 34], we used TIR domain-containing proteins to challenge the ytpGFP system. We chose *Brucella* TIR domain-containing proteins BtpA and BtpB, two divergent translocated effectors involved in establishing the intracellular replication niche [24, 25]. Both have been reported to subvert innate immune signaling by interaction with mammalian TIR domains in diverse ways [18–21, 23, 26, 35].

In the ytpGFP system, homotypic BtpA-BtpA and BtpB-BtpB interactions were much more efficient than heterotypic ones, but also hinted the promiscuity of the TIR fold, as interkingdom interactions, although also weaker than the homotypic ones, were detected between both bacterial TIR domains and all human TIR adaptor proteins downstream TLR4 in LPS-induced innate immune signaling. Furthermore, our data suggest that the divergent non-TIR N-terminal domains of these proteins act to limit the ability of the TIR domains to interact, since in general their TIR domains alone produced more robust interactions than the full-length proteins. We also detected weak BtpA-BtpB heterotypic interactions, especially when the released TIR domain of BtpB was tested. So far, no reports have addressed putative interactions between these two effectors, so it remains to be studied whether they may play a cooperative role in the physiological conditions of *Brucella* intracellular niche within the host.

Although BtpA has been reported to interact with myddosome adaptors by different means [18–20, 22, 24, 36], there is certain controversy in literature on the putative targets of BtpA in the myddosome. Interactions of BtpA with both TIRAP and MyD88 have been described, but most reports seem to favor a preferent association with TIRAP [18, 35, 36], which contributes to its polyubiquitination and proteosomal degradation [26]. However, counterintuitively, BtpA has also been reported to interact with MyD88 via its DD, instead of through its TIR domain [19]. Our ytpGFP results align with such previous reports and provide further evidence of the ability of this protein to interact with TRAM or TRIF, members of the alternative triffosome SMOC branch in TLR4 signaling. Previous reports failed to detect interaction of BtpA or BtpB with TRAM and TRIF [18, 24], but synthetic BtpA-derived peptides have been shown to block both MyD88- and TRIF-dependent signaling [37]. We have previously shown that, when expressed in yeast, TRAM assembles long filaments associated to the plasma membrane, a behavior that is dependent on its N-terminal myristoylation signal [32]. In our ytpGFP constructs, such N-terminal myristoylation signal is masked by the presence of either the β11 GFP strand or the 3×FLAG-6×His tags. Still, TRAM-BtpA interactions were readily recorded and visualized as cytoplasmic filaments and rings. Given that full-length BtpA does not self-interact forming filaments, we can conclude that TRAM filaments can form even in the absence of a myristoylation signal and recruit BtpA.

The less-studied BtpB had been reported to interact with MyD88, but not with TIRAP, by the yeast two-hybrid system [24]. Consistently, we did not detect interaction of BtpB and TIRAP with the ytpGFP system. However, we found that the BtpB TIR domain alone was recruited to the plasma membrane by TIRAP. This underscores the idea that the N-terminal domains of BtpB restrain TIR associations. Nevertheless, it should be considered that, in the yeast two-hybrid assay, nuclear import of the proteins tested is necessary for the detection of interactions, while this is not a requisite for the ytpGFP. Since TIRAP is tightly localized to the plasma membrane in yeast [32], the ytpGFP system should solve interactions involving membrane-bound proteins that would be missed by the classic two-hybrid setting. Overall, our data are compatible with the idea that both BtpA and BtpB TIR domains are susceptible to be recruited by TIRAP to the plasma membrane, where in the scenario of infection they should interfere with MyD88 recruitment, as suggested by previous reports [20, 36].

Our data also suggest that it should be important to systematically assay interaction of both Nt and Ct fusions to the proteins under study. For instance, Nt fusions to TIRAP failed to detect interactions, while Ct fusions did work. It is likely that locating the GFP β-sheet close to the N-terminal plasma membrane-interacting domain of TIRAP topologically isolates it from its TIR domain, hampering GFP reconstitution. On the other hand, Ct fusions of TRIF failed to detect interactions that were positive when Nt fusions were used. We cannot discard topology issues, but we rather hypothesize that, in this case, fusions with the GFP β-strand may interfere with TRIF's C-terminal RHIM domain, which may be important for the proper function of the protein.

A caveat of the ytpGFP system may be its specificity. Some of the interactions here described, especially the heterotypic and interkingdom ones, can be visualized at the fluorescence microscope but do not produce a fluorescent signal strong enough to be detected by flow cytometry. Given that we are using the *GAL1* strong promoter to induce heterologous gene expression, we may be overestimating weak interactions that may not occur physiologically. Considering this, we defined a color code to distinguish those interactions that were robust by both microscopy and cytometry (on a yellow to green scale) from those that were only detected at the microscope. This semiquantitative readout should be useful to use the ytpGFP system for structure-function or pharmacologic studies in the future, by assessing respectively the influence of point mutations or chemical compounds on a given pair which displays a strong interaction.

To summarize, we provide a versatile platform to systematically test protein-protein interactions coupled to subcellular localization of the resulting complexes. We made use of this system to conclude that *Brucella abortus* Btp TIR domains can interact with all human TIR adaptors *in vivo*, an effect which may have been understated in previous reports, and that their N-terminal extensions modulate the availability of the TIR domains for both homo- and heterotypic interactions.

Methods

Strains, culture media and growth conditions

Construction of the AF1 strain (*MATa ura3-52 lys2-801 amber ade2-101 ochre trp1-Δ63 his3-Δ200 leu2-Δ1 HO::GAL1-GFP(β1–9)-kanMX4*) was recently described [33]. Briefly, the *GAL1-GFP(β1–9)-kanMX4* cassette was amplified by PCR from the pGF-IVL794 [7] and integrated upstream of the HO gene start codon in the YPH499 yeast strain [38] by homologous recombination.

Liquid or solid (2% w/v agar) media used were LB (1% w/v bactotryptone, 0.5% w/v yeast extract, and 0.5% w/v NaCl), for *E. coli*, adding the necessary antibiotic for plasmid selection. For yeast growth and transformant selection, Synthetic Dextrose (SD) medium 2% w/v glucose, 0.1% w/v nitrogen base for yeast (Difco), 0.5% ammonium sulphate, and 0.19% of amino acids mix (Formedium) lacking the amino acids necessary for plasmid selection when appropriated. Synthetic Raffinose (SR) and Synthetic Galactose (SG), same formula as SD but substituting glucose by these sugars, were used as pre-

induction and induction media respectively to relief catabolic repression by glucose and activate the *GAL1* promoter for gene expression when necessary.

S. cerevisiae was grown at 30°C in agitation (180 rpm). Strains transformed with plasmids under the control of *GAL1* promoter were inoculated in SR medium overnight. Then, OD600 was adjusted to 0.3 in fresh SG liquid medium and cultures were incubated for 4h.

MoClo cloning

Plasmids used in this work are described in Supplementary Table S1. We made use of the MoClo cloning as described by Lee *et al*. [8]. PCR reactions were performed with the Advantage HD Polymerase enzyme (Takara Bio Inc. RRID: SCR_021372). The NEB Golden Gate Assembly Kit (*BsmB*I-v2; New England Biolabs RRID: SCR_013517) was used to assemble Part plasmids with additional steps at 60°C for 10 min and 80°C for 10 min. PCR primers used are listed in Supplementary Table S2. After verification by Sanger sequencing of the Part plasmids, the final expression plasmids were assembled using the *Bsa*I HF-v2 kit (New England Biolabs RRID: SCR_013517). *Not*I digestion was performed to verify the clones. Coding sequences (CDS) cloned via the MoClo system were checked for the presence of *Bsa*I, *Bsm*BI, and *Not*I restriction sites, which were removed prior to cloning using the method described by [39]. GFP β-strands 10 and 11 sequences containing 5' extensions with restriction sites for *BsaI* and *BsmBI* were synthesized by GenScript (RRID:SCR_002891) and subcloned in Part plasmids 3a and 4a. All TIR protein-encoding genes were assembled as Part plasmids 3b. Empty vectors were assembled using as Part plasmid 3b a short sequence encoding the 3xFLAG-6xHis tags.

Fluorescence microscopy

Microscopy of live yeast cells was performed in a Leica DMi8 Microscope (Leica Microsystems, RRID: SCR_026672) equipped with a Leica K8 charge-coupled device camera and then processed by ImageJ software (RRID: SCR_003070). Yeast cells were cultured overnight in selective SR medium and then refreshed in selective SG medium to adjust OD600nm to 0.3. After 4h at 30ºC, cells suspensions were mounted on slides for live microscopy observation.

Immunodetection of proteins in yeast lysates by Western blotting

Protein expression from all plasmids constructed was confirmed by Western blotting. Yeast cultures were collected on ice in cold Falcon tubes, centrifuged to eliminate any remaining medium and resuspended in 150 µl of ice-cold lysis buffer (50 mM TrisHCl pH = 8, 10%[v/v] glycerol, 1% [v/v] TritonX-100, 0.1%[w/v] SDS, 150 mM NaCl, 50 mM NaF, 1 mM sodium orthovanadate, 50 mM β-glycerolphosphate, 5 mM sodium pyrophosphate, 5 mM EDTA pH = 8 and protease inhibitors) at 4°C in Eppendorf tubes. The protein extracts were obtained through mechanical rupture by glass beads (Sartorius) in a Fastprep-24 system (RRID: SCR_018599), two 30s cycles at 5.5 m/s. The protein concentration of the supernatants was measured at 280 nm in a spectrophotometer Beckman DU 640

(RRID: SCR_008940) and normalized with loading buffer 2· (Tris-HCl 0.1 M pH = 6.8, 20% [v/v] glycerol, 4% [w/v] SDS, bromophenol blue and 10% DTT 1M). The extracts were finally boiled and loaded into a SDS-PAGE get, to be transferred to nitrocellulose membranes by standard techniques. The primary antibodies used were rabbit anti-G6PDH (Sigma- Aldrich, Cat. No. A9521, RRID: SCR_008988, dilution 1:50,000), mouse anti-FLAG (Sigma-Aldrich, Cat. No. F3165, RRID: SCR_008988, dilution 1:1000) and mouse anti-6xHis (Thermo Fisher Scientific, Cat# MA1-21315-D800, RRID: AB_2536988, dilution 1:1000). The secondary antibodies used were IRDye 800LT Goat anti-Mouse IgG (LI-COR Biosciences, Cat. No. 926-32210, RRID: SCR_013430, dilution 1:50,000) and IRDye 680CW Goat anti-Rabbit IgG (LI-COR Biosciences, Cat. No. 926-32211, RRID: SCR_013430, dilution 1:50,000).

Flow Cytometry

Cells were cultured as previously stated and analyzed using a BD FACSCalibur Flow Cytometry System (RRID: SCR_000401), which has a 488 nm excitation laser, a 530/30 band pass emission filter (FL1). At least 10,000 cells were analysed for each experiment. Data were processed using FlowJo software (*BD Biosciences*, RRID: SCR_008520).

Alphafold predictions

Protein structural models were generated using Alphafold 3 [40] through AlphaFold Server (RRID:SCR_025885), both for individual models and multi-protein complexes. To predict structural models, the primary amino acid sequence of the target protein was entered in the “Input” field, omitting the stop codon and any non-amino acid characters. Standard conditions were used for predictions. Standard configuration and auto seed were selected for running the predictions. AlphaFold server generated five ranked structural models determined by quality metrics, labelled as “model_0”, “model_1”, “model_2”, “model_3” and “model_4”. Only the top-ranked models were used in this study. The resulting CIF files were visualized and processed using UCSF ChimeraX (RRID:SCR_015872).

Declarations

Author contributions statement

A.F.-V., M.M. and V.J.C. contributed to the design of the study. All material preparation, data collection and analyses were performed by A.F.-V. with the assistance of E.dV and J.M.C.-S, under the supervision of M.M., I.R.-E. and V.J.C. The manuscript was written by A.F.-V. and V.J.C., then revised and edited by all authors. M.M., H.M., and V.J.C. were responsible for funding acquisition and project administration. All authors have read and approved the manuscript.

Additional Information

The authors declare no competing interests.

Funding

This research is part of the I + D+i Grant PID2022-138591NB-I00, funded by MCIN/AEI/10.13039/501100011033 (Ministerio de Ciencia e Innovación, Spain). A.F.-V. was supported by a research assistant contract PEJ-2021-AI/BMD-21971 from Comunidad de Madrid, and a predoctoral contract from Universidad Complutense de Madrid (UCM)-Santander.

Author Contribution

A.F.-V., M.M. and V.J.C. contributed to the design of the study. All material preparation, data collection and analyses were performed by A.F.-V. with the assistance of E.dV and J.M.C.-S, under the supervision of M.M., I.R.-E. and V.J.C. The manuscript was written by A.F.-V. and V.J.C., then revised and edited by all authors. M.M., H.M., and V.J.C. were responsible for funding acquisition and project administration. All authors have read and approved the manuscript.

Acknowledgement

We are grateful to Suzana Salcedo (University of Wisconsin, WI, USA), Daniel Fisch and Jonathan C. Kagan (Boston Children's Hospital, Boston, MA, USA) for scientific discussion. We are in debt to Jeremy W. Thorner (University of California at Berkeley, USA) for his constant support and for sharing materials developed in his lab by Dr. Gregory C. Finnigan. We also wish to acknowledge the staff at the Genomics Core Unit at the Complutense University of Madrid (UCM) for sequencing and to the UCM Flow Cytometry and Fluorescence Microscopy Unit. We also wish to acknowledge all members of Research Unit 3 at the Dpt. of Microbiology and Parasitology (UCM) for discussion and continuous support.

Data Availability

All data supporting the findings of this study are available within the paper and its Supplementary Information.

References

1. Gaikani, H. K., Stolar, M., Kriti, D., Nislow, C. & Giaever, G. From beer to breadboards: yeast as a force for biological innovation. *Genome Biol.* **25**, 10 (2024).
2. Maneira, C., Chamas, A. & Lackner, G. Engineering *Saccharomyces cerevisiae* for medical applications. *Microb. Cell. Factories*. **24**, 12 (2025).
3. Fields, S. & Sternglanz, R. The two-hybrid system: an assay for protein-protein interactions. *Trends Genet.* **10**, 286–292 (1994).

4. Parrish, J. R., Gulyas, K. D. & Finley, R. L. Yeast two-hybrid contributions to interactome mapping. *Curr. Opin. Biotechnol.* **17**, 387–393 (2006).
5. Pedelacq, J. D. & Cabantous, S. Development and Applications of Superfolder and Split Fluorescent Protein Detection Systems in Biology. *Int. J. Mol. Sci.* **20**, 3479 (2019).
6. Cabantous, S. et al. A new protein-protein interaction sensor based on tripartite split-GFP association. *Sci. Rep.* **3**, 2854 (2013).
7. Finnigan, G. C., Duvalyan, A., Liao, E. N., Sargsyan, A. & Thorner, J. Detection of protein–protein interactions at the septin collar in *Saccharomyces cerevisiae* using a tripartite split-GFP system. *Mol. Biol. Cell.* **27**, 2708–2725 (2016).
8. Lee, M. E., DeLoache, W. C., Cervantes, B. & Dueber, J. E. A Highly Characterized Yeast Toolkit for Modular, Multipart Assembly. *ACS Synth. Biol.* **4**, 975–986 (2015).
9. Kagan, J. C., Magupalli, V. G. & Wu, H. SMOCs: supramolecular organizing centres that control innate immunity. *Nat. Rev. Immunol.* **14**, 821–826 (2014).
10. Luo, L., Lucas, R. M., Liu, L. & Stow, J. L. Signalling, sorting and scaffolding adaptors for Toll-like receptors. *J. Cell. Sci.* **133**, jcs239194 (2020).
11. Watters, T. M., Kenny, E. F. & O'Neill, L. A. J. Structure, function and regulation of the Toll/IL-1 receptor adaptor proteins. *Immunol. Cell. Biol.* **85**, 411–419 (2007).
12. Essuman, K. et al. TIR Domain Proteins Are an Ancient Family of NAD+-Consuming Enzymes. *Curr. Biol.* **28**, 421–430e4 (2018).
13. Wani, K. A. & Pukkila-Worley, R. Evolutionarily ancient functions of enzymatic TIR proteins in innate immunity. *Trends Immunol.* **46**, 441–454 (2025).
14. Askarian, F. et al. A *Staphylococcus aureus* TIR Domain Protein Virulence Factor Blocks TLR2-Mediated NF-κB Signaling. *J. Innate Immun.* **6**, 485–498 (2014).
15. Imbert, P. R. et al. A *Pseudomonas aeruginosa* TIR effector mediates immune evasion by targeting UBAP 1 and TLR adaptors. *EMBO J.* **36**, 1869–1887 (2017).
16. Yadav, M. et al. Inhibition of TIR domain dignaling by TcpC: MyD88-dependent and independent effects on *Escherichia coli* virulence. *PLoS Pathog.* **6**, e1001120 (2010).
17. Yu, H., Gu, X., Wang, D. & Wang, Z. Brucella infection and Toll-like receptors. *Front. Cell. Infect. Microbiol.* **14**, 1342684 (2024).
18. Alaidarous, M. et al. Mechanism of bacterial interference with TLR4 signaling by *Brucella* Toll/Interleukin-1 Receptor domain-containing protein TcpB. *J. Biol. Chem.* **289**, 654–668 (2014).
19. Chaudhary, A. et al. The *Brucella* TIR-like protein TcpB interacts with the death domain of MyD88. *Biochem. Biophys. Res. Commun.* **417**, 299–304 (2012).
20. Cirl, C. et al. Subversion of Toll-like receptor signaling by a unique family of bacterial Toll/interleukin-1 receptor domain–containing proteins. *Nat. Med.* **14**, 399–406 (2008).
21. Jakka, P., Namani, S., Murugan, S., Rai, N. & Radhakrishnan, G. The *Brucella* effector protein TcpB induces degradation of inflammatory caspases and thereby subverts non-canonical inflammasome

activation in macrophages. *J. Biol. Chem.* **292**, 20613–20627 (2017).

22. Li, W. et al. *Brucella* TIR-like protein TcpB/Btp1 specifically targets the host adaptor protein MAL/TIRAP to promote infection. *Biochem. Biophys. Res. Commun.* **477**, 509–514 (2016).
23. Radhakrishnan, G. K., Yu, Q., Harms, J. S. & Splitter, G. A. Brucella TIR Domain-containing Protein Mimics Properties of the Toll-like Receptor Adaptor Protein TIRAP. *J. Biol. Chem.* **284**, 9892–9898 (2009).
24. Salcedo, S. P. et al. BtpB, a novel *Brucella* TIR-containing effector protein with immune modulatory functions. *Front Cell. Infect. Microbiol* **3**, (2013).
25. Salcedo, S. P. et al. *Brucella* Control of Dendritic Cell Maturation Is Dependent on the TIR-Containing Protein Btp1. *PLoS Pathog.* **4**, e21 (2008).
26. Sengupta, D. et al. Subversion of Innate Immune Responses by *Brucella* through the Targeted Degradation of the TLR Signaling Adapter, MAL. *J. Immunol.* **184**, 956–964 (2010).
27. Snyder, G. A. et al. Molecular mechanisms for the subversion of MyD88 signaling by TcpC from virulent uropathogenic *Escherichia coli*. *Proc. Natl. Acad. Sci. U. S. A.* 110, 6985–6990 (2013).
28. Cabantous, S. et al. A New Protein-Protein Interaction Sensor Based on Tripartite Split-GFP Association. *Sci. Rep.* **3**, 2854 (2013).
29. Lee, M. E., DeLoache, W. C., Cervantes, B. & Dueber, J. E. A Highly Characterized Yeast Toolkit for Modular, Multipart Assembly. *ACS Synth. Biol.* **4**, 975–986 (2015).
30. Kaplan-Türköz, B. et al. Structure of the Toll/interleukin 1 receptor (TIR) domain of the immunosuppressive *Brucella* effector BtpA/Btp1/TcpB. *FEBS Lett.* **587**, 3412–3416 (2013).
31. Coronas-Serna, J. M. et al. The TIR-domain containing effectors BtpA and BtpB from *Brucella abortus* impact NAD metabolism. *PLoS Pathog.* **16**, e1007979 (2020).
32. Coronas-Serna, J. M., del Val, E., Kagan, J. C., Molina, M. & Cid, V. J. Heterologous expression and assembly of human TLR signaling components in *Saccharomyces cerevisiae*. *Biomolecules* **11**, 1737 (2021).
33. Del Val, E., Fernández-Vega, A., Molina, M. & Cid, V. J. MyD88 polymerization and association to cellular membranes in a yeast heterologous model. *Cell. Mol. Life Sci. CMLS.* **82**, 288 (2025).
34. Ve, T., Williams, S. J. & Kobe, B. Structure and function of Toll/interleukin-1 receptor/resistance protein (TIR) domains. *Apoptosis* **20**, 250–261 (2015).
35. Li, J. et al. BtpB inhibits innate inflammatory responses in goat alveolar macrophages through the TLR/NF-κB pathway and NLRP3 inflammasome during *Brucella* infection. *Microb. Pathog.* **166**, 105536 (2022).
36. Snyder, G. A. et al. Crystal Structures of the Toll/Interleukin-1 Receptor (TIR) Domains from the Brucella Protein TcpB and Host Adaptor TIRAP Reveal Mechanisms of Molecular Mimicry. *J. Biol. Chem.* **289**, 669–679 (2014).
37. Ke, Y. et al. Inhibition of TLR4 signaling by *Brucella* TIR-containing protein TcpB-derived decoy peptides. *Int. J. Med. Microbiol.* **306**, 391–400 (2016).

38. Sikorski, R. S. & Hieter, P. A system of shuttle vectors and yeast host strains designed for efficient manipulation of DNA in *Saccharomyces cerevisiae*. *Genetics* **122**, 19–27 (1989).
39. Marillonnet, S. & Grützner, R. Synthetic DNA assembly using Golden Gate cloning and the hierarchical modular cloning pipeline. *Curr. Protoc. Mol. Biol.* **130**, e115 (2020).
40. Abramson, J. et al. Accurate structure prediction of biomolecular interactions with AlphaFold 3. *Nature* **630**, 493–500 (2024).

Figures

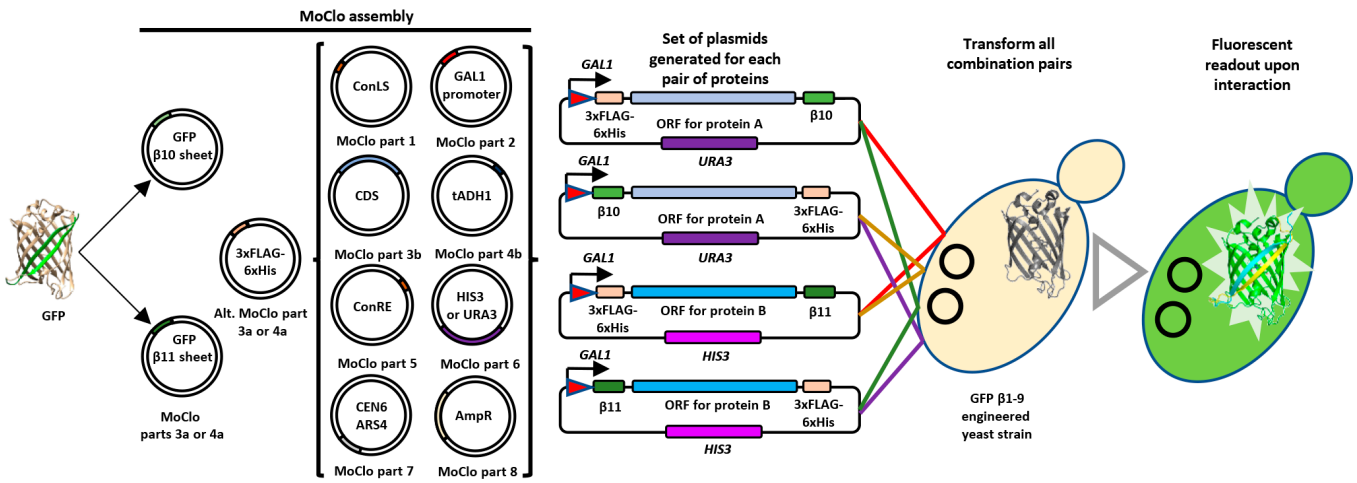


Figure 1

sequences coding the β10 and β11 sheets of GFP were cloned in the 3a or 4a part vectors of the MoClo system to produce N-terminal and C-terminal fusions, respectively, and combined with the alternative 3´FLAG-6´His 3a or 4a part vectors to tag the protein with immunodetectable epitopes in the other end. By combining the part plasmids with the desired combination of part vectors, centromeric expression vectors were assembled in which the desired coding sequence (CDS) cloned in the 3b part vector was either C- or N-terminally fused to 3´FLAG-6´His and GFP-β10 on *URA3*-based vectors or to 3´FLAG-6´His and GFP-β11 on *HIS3*-based vectors, both to be expressed from the galactose-dependent *GAL1* promoter. Co-transformation of *URA3* and *HIS3* plasmid combinations in the AF1 strain, bearing an integrated GAL1-GFP-β(1-9) cassette, allows testing interaction of all pair combinations (colored lines) of N-terminal and C-terminal fusions. Reconstitution of GFP, detected by fluorescent signal, accounts for interaction of the fusions tested, providing information of the subcellular localization where the interaction takes place.

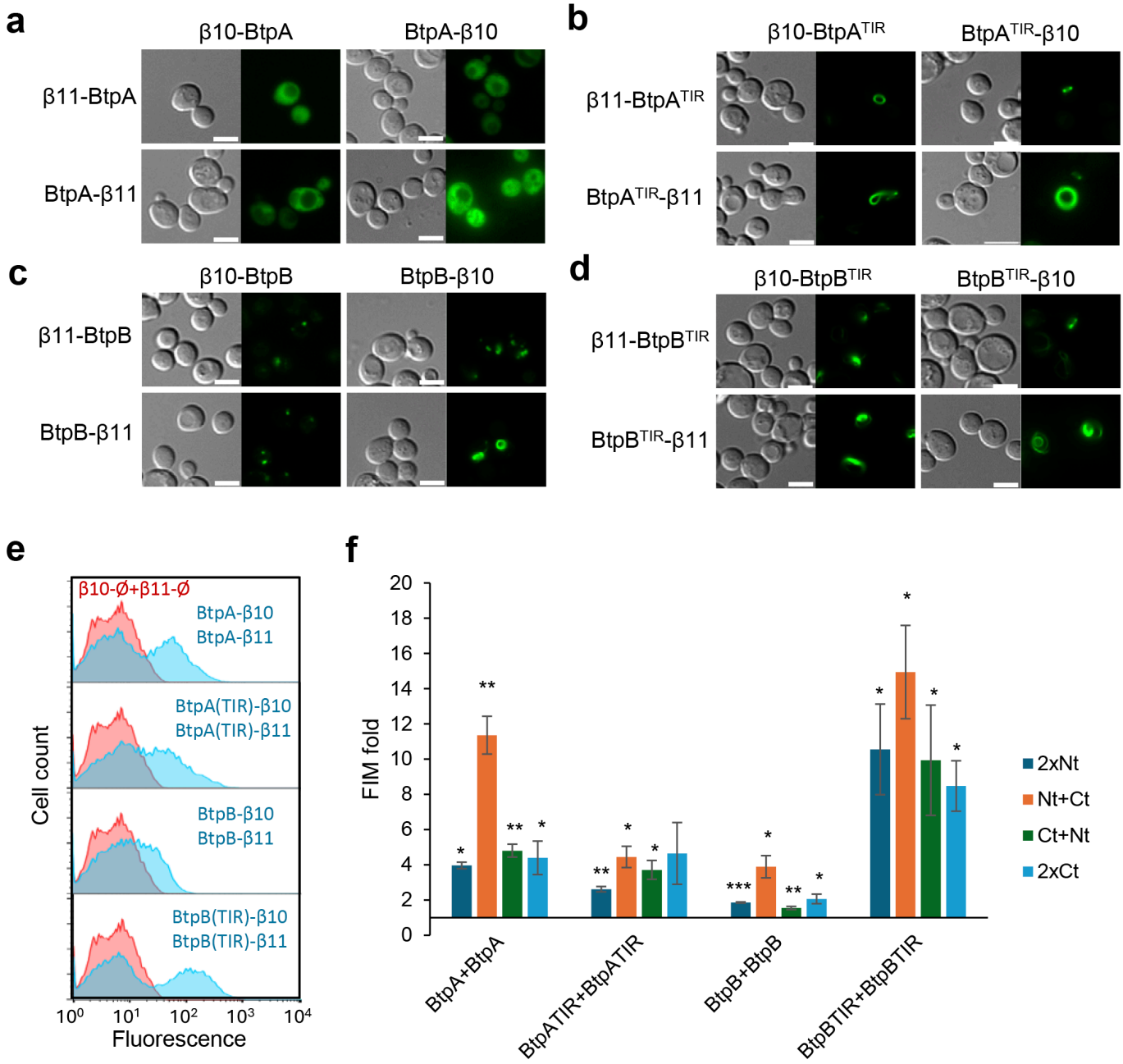


Figure 2

Study of BtpA and BtpB homotypic interactions both in the presence and absence of their N-terminal non-TIR domains. **A-D.** Representative bright field and green fluorescence images of all combinations of self-interactions for BtpA (**A**), BtpA(TIR) (**B**), BtpB (**C**), and BtpB(TIR) (**D**). As indicated, in each panel, combinations with both β-strands at Nt (2×Nt), Nt-Ct, Ct-Nt, and Ct-Ct (2×Ct) are represented in the first, second, third and fourth quarter, respectively. In all cases the point mutations BtpA^{E217A} or BtpB^{E234A} were present to elude TIR toxicity in yeast. AF1 yeast strain was co-transformed with the combination of GFP β10 and β11 strand plasmids, as indicated, and incubated for 4 h in SG galactose-based medium

before microscopic visualization. Bars represent 5 µm. **D.** Representative flow cytometry histograms of all homotypic BtpA or BtpB 2×Ct combinations, indicated in blue, compared to the basal signal of the control bearing empty vectors (red). **F.** Quantification of fluorescence intensity mean (FIM) of all ytpGFP pairs as in A-D, represented as a ratio relative to the basal signal of the empty plasmid control (FIM fold). Data in the graph are the average of three experimental replicates on three different transformant clones. Histograms in E illustrate a representative experiment of the 2×Ct set, shown in blue bars in the graph. Error bars represent the standard deviation (SD). Asterisks indicate a p value <0.05 (*), <0.01 (**), or <0.001 (***) calculated using Student's t test.

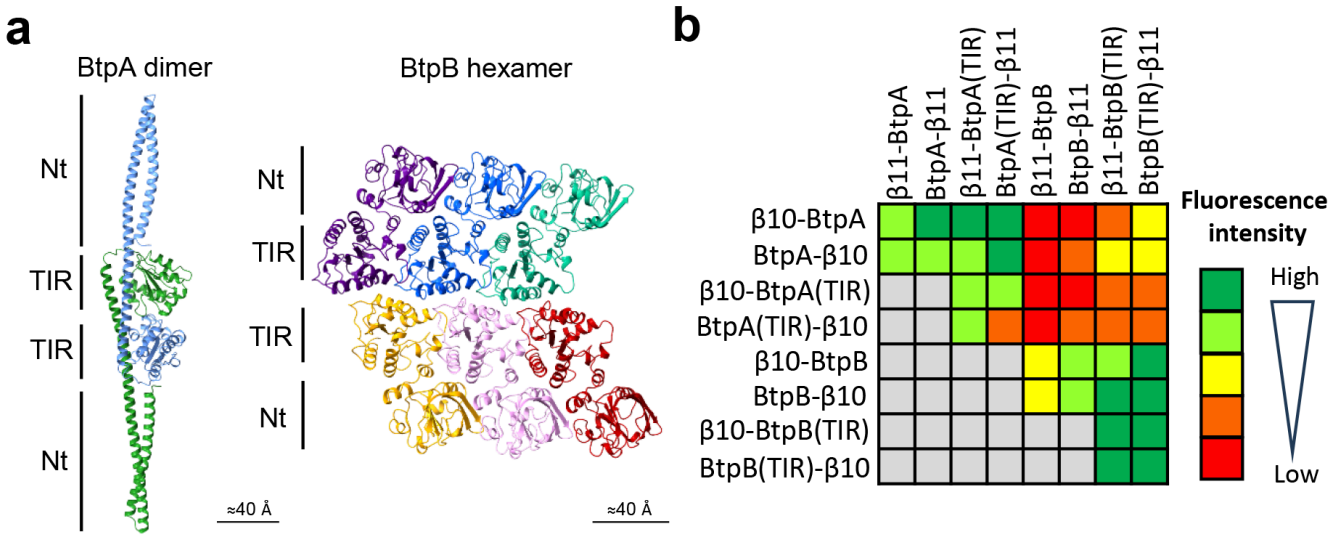


Figure 3

A. Alphafold3 structure predictions of a BtpA dimer (left) and a BtpB hexamer (right). Each protein subunit in the complex is marked in a different color. Scale bars correspond to 40 Å. **B.** Grid showing the combinations tested and the outcome of interactions according to the following color code: green, strong signal at the fluorescence microscope and over 5-fold fluorescence intensity mean (FIM; p<0.05) over vector alone control in flow cytometry; light green, strong signal at the fluorescence microscope and 2- to 5-fold FIM (p<0.05) over vector alone control in flow cytometry; yellow, moderate signal at the fluorescence microscope and <2-fold FIM (p<0.05) over vector alone control in flow cytometry; orange, low signal at the fluorescence microscope and <2-fold FIM, not statistically significant over negative control in flow cytometry; red, no signal at fluorescence microscopy; gray, not determined .

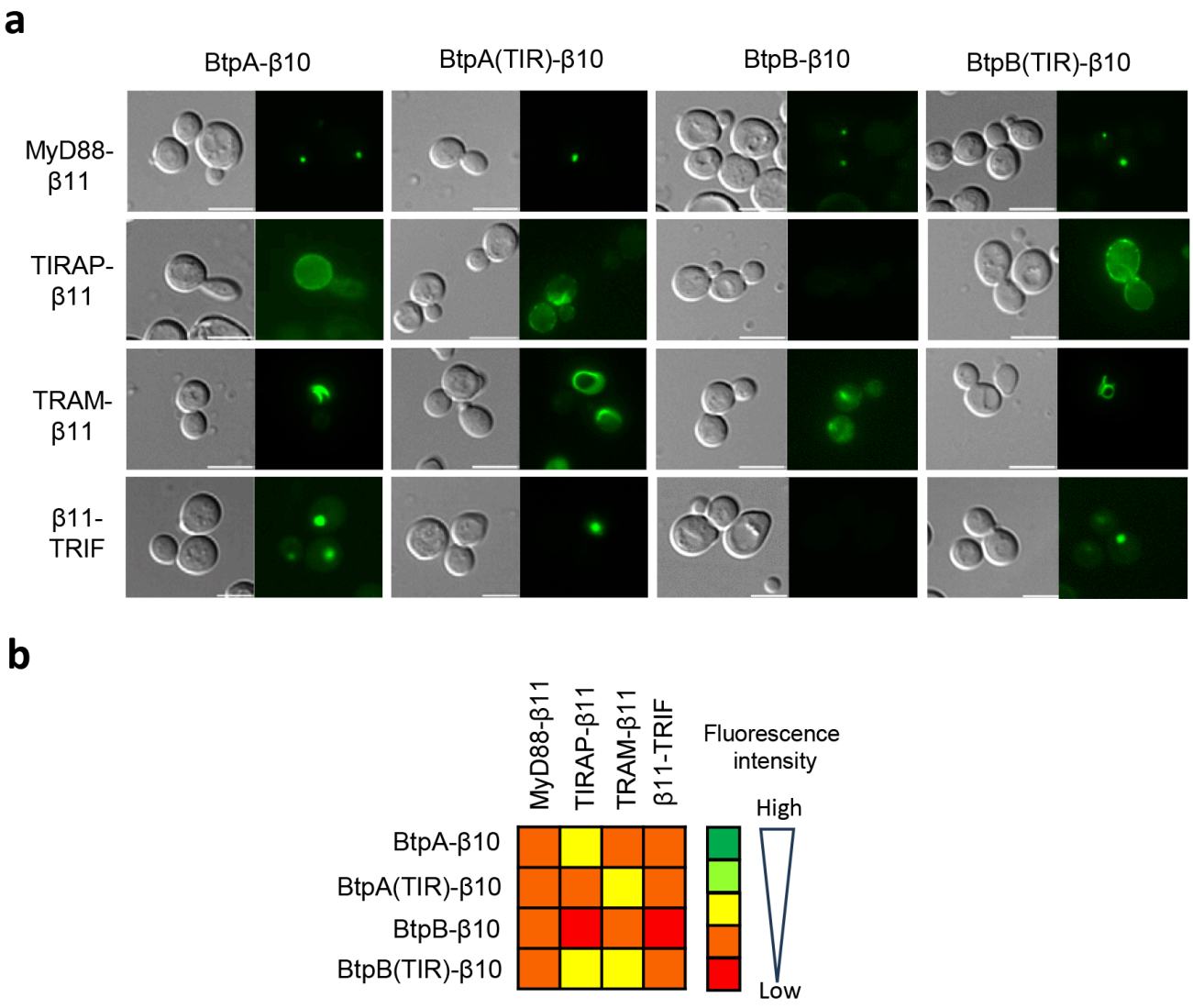


Figure 4

Study of interkingdom BtpA and BtpB interactions with human TIR-containing innate immune signaling adaptors. **A.** Representative bright field and their respective green fluorescence images of cells displaying the indicated interactions. Only C-terminal (tail-tail) fusions are shown, except for TRIF, in which images from the head-tail conformation are shown, given that the all tail-tail interactions for TRIF were negative. For all combinations see Supplementary Figure S4. *S. cerevisiae* strain and manipulation of transformants was as in Figure 2. Bars represent 5 μm. **B.** Grid showing the efficiency of interaction of the same panel of combinations as in A, integration microscopy data with the corresponding flow cytometric analyses (see Supplementary Figure S5). To interpret the color code, see Figure 3B.

Supplementary Files

This is a list of supplementary files associated with this preprint. Click to download.

- SupplementaryFiguresandtablesfinal10M.pdf